Radiative-convective model of warming Mars with artificial greenhouse gases

Margarita M. Marinova[1] and Christopher P. McKay
NASA Ames Research Center, Moffett Field, California, USA

Hirofumi Hashimoto
Institute of Engineering Mechanics and Systems, University of Tsukuba, Tsukuba, Japan

Received 13 June 2004; accepted 14 December 2004; published 10 March 2005.

[1] Artificial greenhouse gases could be used to warm Mars in order to make it habitable. Here we present new laboratory measurements of the thermal infrared absorption spectra of seven artificial greenhouse gases (CF_4, C_2F_6, C_3F_8, SF_6, CF_3Cl, CF_3Br, CF_2Cl_2) at concentrations from 10^{-7} up to unity. We used a radiative-convective multilayer model to compute the warming caused by a mixture of the four fluorine-based greenhouse gases. The results show that for current Mars, C_3F_8 produces the largest warming: 0.56 K and 33.5 K for partial pressures of 10^{-3} Pa and 1 Pa, respectively. Averaged over partial pressures from 0.01 to 1 Pa, the range of most interest for planetary ecosynthesis, CF_4, C_2F_6, and SF_6 were 17%, 49%, and 48% as effective as C_3F_8, respectively. The optimal mixture of the four fluorine-based greenhouse gases, taking into account the overlapping of their absorption bands, was 16% more effective than pure C_3F_8, averaged over the range 0.01 Pa to 1 Pa. Energy balance calculations suggest that the addition of $\sim$0.2 Pa of the best greenhouse gases mixture or $\sim$0.4 Pa of C_3F_8 would shift the equilibrium to the extent that CO_2 would no longer be stable at the Martian poles and a runaway greenhouse effect would result.

Citation: Marinova, M. M., C. P. McKay, and H. Hashimoto (2005), Radiative-convective model of warming Mars with artificial greenhouse gases, *J. Geophys. Res.*, *110*, E03002, doi:10.1029/2004JE002306.

1. Introduction

[2] Artificial greenhouse gases, commonly chlorine-, bromine-, and fluorine-containing compounds, have been released into Earth's atmosphere for several decades and have reached levels where the warming from these gases could be contributing to the measured warming trend of Earth's climate. Many of these compounds absorb radiation in the wavelength region of 8–12 μm where CO_2 and H_2O, the dominant natural greenhouse gases on the Earth, are not effective absorbers. This absorption in the 8–12 μm "window" region, as well as strong band absorption coefficients, result in some artificial greenhouse gases being thousands of times more effective than CO_2 in greenhouse warming [*Houghton et al.*, 2001]. As a result, there is considerable interest in the radiative properties of these artificial greenhouse gases and their effect on the radiation balance of the atmosphere [*Ramanathan et al.*, 1985; *Houghton et al.*, 2001; *Hansen et al.*, 1989; *Rodhe*, 1990; *Roehl et al.*, 1995]. It has also been suggested that artificial greenhouse gases could be used to warm Mars as the first step in restoring a biosphere on that planet [*Lovelock and Allaby*, 1984; *McKay et al.*, 1991; *Marinova et al.*, 2000; *Gerstell et al.*, 2001]. The levels of artificial greenhouse gases in Earth's atmosphere are currently about 1300 ppt [*Houghton et al.*, 2001]; much higher levels would be required to warm Mars enough to support life.

[3] Warming Mars and increasing its atmospheric pressure are the key requirements for making the planet suitable for life. Of the proposed warming methods [*Fogg*, 1995], the use of artificial greenhouse gases to increase the surface temperature is probably the most efficient and the only currently technically feasible approach [*McKay et al.*, 1991; *Marinova et al.*, 2000]. *McKay et al.* [1991] suggested that an important step in the process is warming the atmosphere to the point that any polar CO_2 deposits become unstable and evaporate completely. The total amount of frozen CO_2 in the Martian polar caps (especially the southern cap) is uncertain and may not be enough to significantly increase the pressure on Mars [*Mellon*, 1996; *Byrne and Ingersoll*, 2003] (but cf. *Jakosky et al.* [1995]). Nevertheless, it is of interest to consider the stability of polar CO_2 ice in response to atmospheric warming. Figure 1 shows the pressure-temperature equilibrium curve for CO_2 ice as a function of atmospheric CO_2 pressure (adapted from *McKay et al.* [1991]), and the polar temperature as a

[1]Now at California Institute of Technology, Pasadena, California, USA.

Copyright 2005 by the American Geophysical Union.
0148-0227/05/2004JE002306$09.00

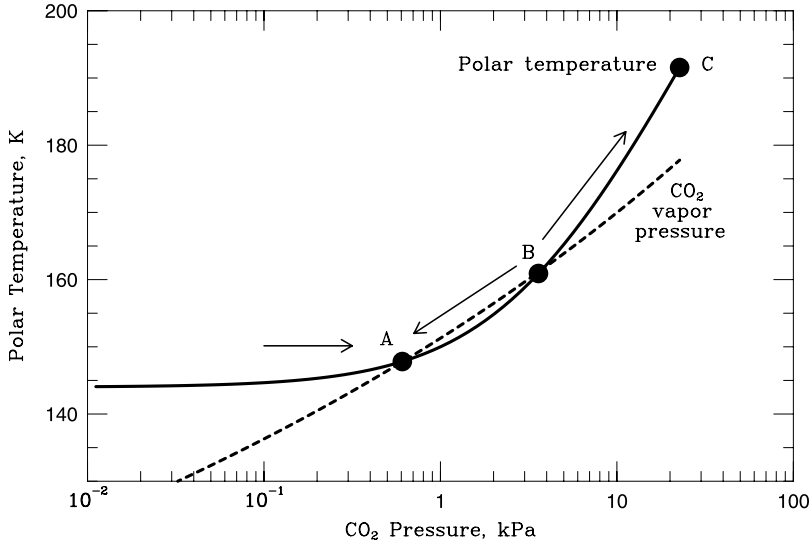

Figure 1. The CO_2 vapor pressure and polar temperature as a function of atmospheric CO_2 pressure. Point A (current state) is stable, and perturbations about this point will tend to drive the system back to point A. Point B is unstable: values below point B will return to point A, while values above point B will tend to go to point C, that is, the runaway greenhouse state.

function of atmospheric pressure (from results by *Pollack et al.* [1987] and *Gierasch and Toon* [1973] described later in more detail). For an equilibrium to persist, the pressure and temperature of the ice must be in agreement with the temperature and pressure determined by the greenhouse effect. At low temperatures such an equilibrium exists, labeled point A in Figure 1. As the temperature increases another point is reached, labeled B, at which the curves cross, but unlike A, point B is not a stable equilibrium. Points below B will move toward A, and points above B will move to the right until the entire available CO_2 reservoir has evaporated into the atmosphere. Figure 1 shows that in order for Mars to enter a self-sustaining runaway greenhouse effect, Mars' poles, presently at point A, must be warmed approximately 20 K. Release of CO_2 from the polar regolith follows similar stability and dynamics [*McKay et al.*, 1991].

[4] If artificial greenhouse gases are used to warm Mars, then compounds containing chlorine or bromine would not be desirable because both elements catalytically destroy ozone. Fluorine-based compounds (e.g., SF_6 and perfluorocarbons) are therefore of particular interest for the warming of Mars. In addition, it would be desirable to have gases with a strong greenhouse effect and a long lifetime. For practical reasons, the gases must be composed of elements readily available on the Martian surface. In this study we have focused our modeling efforts on four gases that satisfy these criteria: CF_4, C_2F_6, C_3F_8, and SF_6. The relative global warming potential (GWP, with respect to CO_2) of these compounds in Earth's present atmosphere are estimated to be 5700, 11900, 8600, and 22200, respectively [*Houghton et al.*, 2001], and they have extremely long lifetimes in Earth's atmosphere: 50000, 10000, 2600, and 3200 years, respectively [*Houghton et al.*, 2001]. On Mars, these lifetimes may be longer due to the reduced solar flux reaching Mars, but might be shorter due to the less effective UV shielding of the CO_2 atmosphere compared to the O_2 and O_3 in Earth's atmosphere. Accurately estimating the lifetime of these gases on Mars is difficult (as it is on Earth). For example SF_6 is discussed by *Ko et al.* [1993]; it may not be destroyed by UV that penetrates the Martian CO_2 (>200 nm), but may be destroyed by electron capture and ion reactions. *Ramanathan et al.* [1985] state that for CF_4, C_2F_6, and SF_6 (and presumably for C_3F_8), the loss rate is due to extreme UV and electron capture removal in the ionosphere. In this case the lifetimes on Mars could be much longer than on Earth due both to the reduced solar flux and the absence of a magnetosphere. A detailed analysis of the lifetimes of these gases on Mars remains to be done.

[5] Figure 2 shows the thermal infrared wavelengths and the absorption bands of the four artificial greenhouse gases considered here, as well as the absorption regions for CO_2 and H_2O. Thick, medium thick, and thin lines represent strong, medium, and weak bands, respectively. Note that the strength of the CO_2 bands are relative to the other CO_2 bands and not to the strength of the super greenhouse gases. No band strength is implied for water vapor. Also shown are the blackbody curves for surface radiation from Earth and Mars. For Mars, the current surface radiation is effectively the same as the radiation from the top of the atmosphere: there is negligible greenhouse warming due to the present atmosphere. For Earth there is a 30 K greenhouse effect. If the surface temperature of Mars were to be the same as Earth's, then the greenhouse warming required to maintain this temperature is the difference between the blackbody curve at 288 K and that at 216 K - a 70 K greenhouse effect.

[6] In this paper we report new Fourier Transform Infra Red (FTIR) measurements of the transmission spectrum of four fluorine-based gases (CF_4, C_2F_6, C_3F_8, and SF_6), as well as three chlorine- and bromine-containing gases (CF_3Cl, CF_3Br, CF_2Cl_2). The absorption bands of the gases were fitted with 3-term exponential fits. The three Cl- and Br-containing gases were not used in the radiative transfer

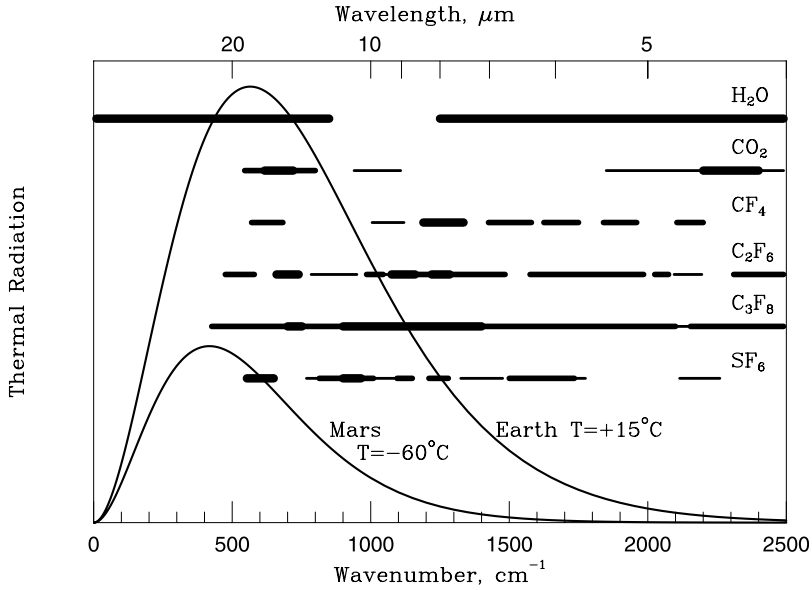

Figure 2. Position of the absorption bands of the fluorine-based compounds that were analyzed, CO_2, and water vapor, with respect to the blackbody radiation curves of Earth and Mars. The thickness of the line represents the strength of the band, with the thick lines representing strong bands and thin lines representing weak bands. For CO_2 the band strength is relative to the other CO_2 bands, and not to the super greenhouse gases. A band strength is not implied for H_2O. Note that C_3F_8 absorbs over most of the spectrum.

calculation; however, we include the spectral band data and fits in this paper (Appendix A). The fluorine-based gases were used in a radiative-convective simulation of the thermal structure of the Martian atmosphere to calculate the warming caused by a greenhouse gas partial pressure up to 10 Pa. The amount of CO_2 in the atmosphere was also varied from 600 to 10^4 Pa. In addition, we computed the effective gray opacity of these compounds as a function of concentration and used this to derive simple formulae for use in climate calculations.

2. Data

[7] Transmission data for all seven artificial greenhouse gases reported here were obtained using a Fourier Transform Infra Red (FTIR) spectrometer (Perkin Elmer 1725X FTIR) over a path length of 10 cm, in a chamber at standard atmospheric temperature and pressure. The column amount in the test cell was similar to the amounts of interest for artificial greenhouse gases calculations (0.7 Pa Mars equivalent). All gases were measured at concentrations of 10^{-7}, 10^{-6}, 10^{-5},... to 10^{0}; the gases were diluted with Argon, which does not have absorption bands in the wavelength interval of interest. The measurements were made for the wave number range 400–4000 cm^{-1} (wavelength range 25–2.5 μm), with a resolution of 1 cm^{-1}. The transmission spectra for C_3F_8 at concentrations of 10^{-6}, 10^{-3}, 10^{-1}, are shown in Figure 3. The data for all gases are available in the online auxiliary material[1].

[8] Absorption bands were identified at each concentration. The concentration at which the width of an absorption feature (band) was defined depended on the band strength. Strong bands were seen at low concentrations and became saturated at high concentrations. At the other extreme, the weakest bands were only discernible at the highest concentration. For each band the concentration which most clearly showed the band feature was used to define the wave number boundaries for that band. These band boundaries were then used in computing the average transmission for the band for all concentrations. Some absorption bands were clearly composed of several spectral features convolved together. The bands were treated as separate only in cases where the absorption decreases (transmission increases) significantly between adjacent peaks (e.g., peaks with transmissions of ~70% are separated by a trough with transmission of ~95%). Given the gas concentrations and path length, the percentage transmission versus column gas amount was computed; these data were then fitted with an exponential sum fit.

[9] To compute the greenhouse effect of CO_2, we considered its three principal absorption regions in the infrared at 545–800, 940–1110, and 1850–2500 cm^{-1}. These were divided into three, three, and five bands, respectively. The transmission in each band was computed using an 8-term *k*-coefficient expression derived from line-by-line calculations for a pressure of 10^3 Pa of CO_2 at 250 K (provided by R. Freedmann, personal communication based on the Ames Mars GCM). These transmission values were then fit with 3-term exponentials, as described below, to reduce computational time. This provided a rough representation of CO_2 absorption which we adjusted to fit previously published results for CO_2 warming on Mars [*Pollack et al.*, 1987], as described in the methods section.

[10] Changes in the absorption bands due to pressure and temperature broadening were not accurately taken into

[1]Auxiliary material is available at ftp://ftp.agu.org/apend/je/2004JE002306.

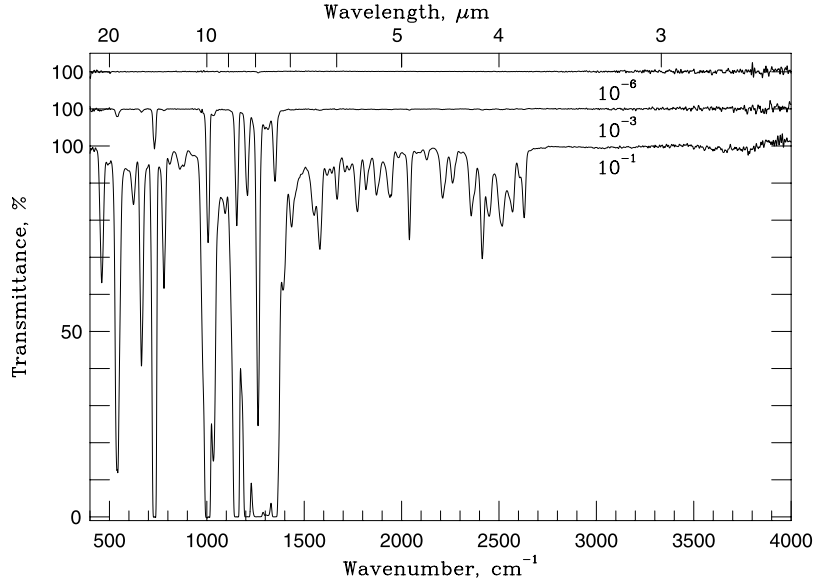

Figure 3. Transmission spectra for C_3F_8 at concentrations of 10^{-6}, 10^{-3}, and 10^{-1}; curves offset for clarity.

account in the calculations. The absorption bands were measured and characterized at standard atmospheric pressure and temperature, and were diluted with Argon. On Mars, the lower temperatures, lower pressures, and dilution by CO_2 would change the strength and shape of the absorption bands. It is expected that the lower temperatures would broaden the absorption bands, but also make them shallower [*Burch et al.*, 1969], likely resulting in a minor net effect [*Roehl et al.*, 1995]. The lower atmospheric pressures would tend to make the bands narrower. Replacing Ar with CO_2 as the broadening gas would tend to increase the strength of the bands by about 30% [*Howard et al.*, 1956; *Burch et al.*, 1969; *Pollack et al.*, 1993].

3. Exponential Fitting

[11] We fitted the average transmission data of each individual band to a sum of exponentials as a function of concentration [*Sun and Rikus*, 1999; *Kratz et al.*, 1998]. The advantage of this form is that the individual terms in the exponential sum can be used directly in radiative transfer calculations even when scattering is included. The combined radiative transfer in the spectral interval is the weighted sum of the individual computations for each term of the exponential sum. In this sense each exponential sum term is treated like a simple monochromatic absorption term following Beer's Law [*Thomas and Stamnes*, 1999]. For simplicity, we used the minimum number of terms necessary to accurately represent the transmission data for any specific band. For all bands we found that an accurate fit could be obtained with three or less terms; the strongest bands were the most difficult to fit and required the most terms. The fits were of the form

$$\mathcal{T} = \sum_{i=1}^{n} a_i e^{-k_i N}, \tag{1}$$

where $\mathcal{T}$ is the transmission, n varies between 1 and 3 depending on what order exponential fit is needed to produce a good fit, a_i is a weighting factor ($\sum_{i=1}^{n} a_i = 1$), k_i is the absorption coefficient in units of m^2 per molecule, and N is the column density of the absorbing gas in molecules m^{-2}. The fitted transmission then describes the average transmission in the band and is assumed to be the transmission for all wavelengths within the band (i.e., the band shape is treated as rectangular). The values of the parameters a and k were chosen to minimize the absolute difference between the fitted and measured transmission. Figure 4 shows examples of strong, medium, and weak bands and the corresponding 3-term, 2-term, and 1-term exponential fits, respectively. All fits had an overall error between the computed and measured transmission values (summated, squared difference) of less than 1%, and the majority of fits had an overall error (summated, squared difference) of less than 0.5%. In the case of CO_2, an error of up to 2.4% was present.

[12] Appendix A (Tables A1–A7) lists all identified bands for the four fluorine-based and three chlorine- and bromine-containing gases that were analyzed, the 3-term exponential fits that were determined, and the intensity for each band. The intensity was calculated as described by *Roehl et al.* [1995] using

$$S = \frac{1}{pl} \int_{\nu_1}^{\nu_2} \ln\left[\frac{I_0(\nu)}{I(\nu)}\right] d\nu, \tag{2}$$

where S is the integrated band intensity [cm^{-1}/cm atm], p is the sample pressure (atm), l is the path length (cm), $I_0(\nu)$ is the intensity transmitted at wave number ν with the cell empty and $I(\nu)$ is the intensity transmitted with the cell full, and ν_1 and ν_2 are the ranges of the band [cm^{-1}]. Our results are in general agreement with those of *Roehl et al.* [1995],

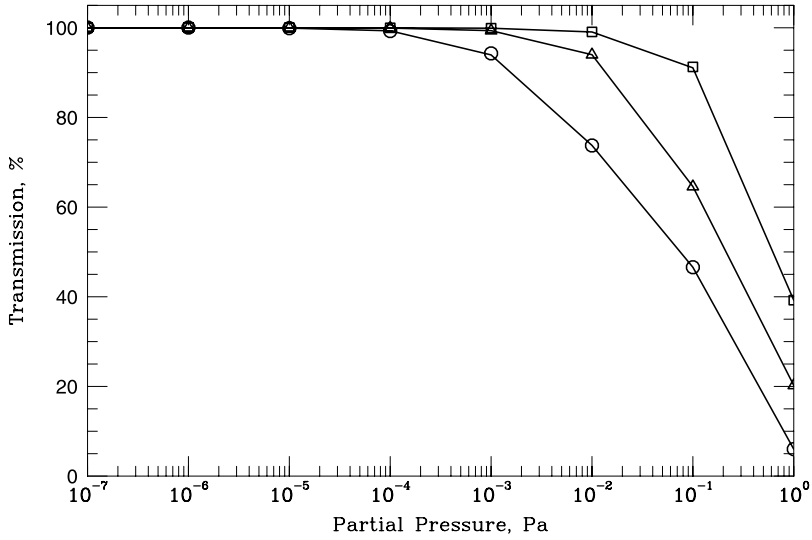

Figure 4. Strong (circles), medium (triangles), and weak (squares) absorption bands fit using 3-term, 2-term, and 1-term exponential fits (solid lines), respectively.

Ko et al. [1993], *Hansen et al.* [1989], and *Varanasi and Chudamani* [1988].

4. Radiative-Transfer Methods

[13] We developed a multilayer nongray radiative-convective transfer computer model to calculate the effect of the addition of artificial greenhouse gases on the surface temperature of Mars. For a given temperature profile, the model computes the upward and downward radiative fluxes throughout the atmosphere, taking into account both CO_2 and greenhouse gas concentrations. The temperature profile is then adjusted until radiative-convective equilibrium is achieved and the surface satisfies the appropriate convective conditions. In this section we describe the model and the temperature adjustment method used in this computation. Because only temperatures less than ~260 K are considered, H_2O opacity was not included in the calculations.

4.1. Radiative-Convective Calculation

[14] Our computational method uses the hemispheric mean two-stream approximation in computing the upward and downward fluxes in the atmosphere [*Meador and Weaver*, 1980; *Toon et al.*, 1989]. The atmosphere is divided into discrete layers. In this approach, the thermal radiation is assumed uniform in the upward and in the downward directions. After integrating over the azimuthal angle, the downward flux (F^-), is given by

$$F^- = 2\pi \int_0^1 I^- \mu \, d\mu, \tag{3}$$

where I^- is the intensity in the downward direction, and $\mu = \cos\theta$ is the projection of the beam onto the z axis. Since we approximate the radiation as uniform in the downward direction, I^- is not a function of μ and equation (3) is evaluated to

$$F^- = \pi I^-. \tag{4}$$

We use the integral form of the radiative transfer equation,

$$I^-(\tau, \bar{\mu}) = I^-(\tau = 0, \bar{\mu})\, e^{-\tau/\bar{\mu}} + \int_0^{\tau} B(\tau', \bar{\mu})\, e^{-(\tau-\tau')/\bar{\mu}}\, d\tau'/\bar{\mu}, \tag{5}$$

where τ is the optical depth, τ' is the variable of integration, $\bar{\mu}$ is the hemispherically averaged incidence angle ($\bar{\mu} = 0.5$ since the radiation is assumed uniform in the downward direction), and B is the Planck function. The first term in equation (5) represents the energy that is transmitted through the layer, while the second represents the energy that has its source in the layer (that is emitted by gas in the layer) and then is attenuated on the way down through the rest of the layer. Additionally, we approximated the Planck function as a linear function of τ [*McKay et al.*, 1989], so that

$$B = B_0 + \tau B_1. \tag{6}$$

B_0 and B_1 can be solved for by setting the top of the layer ($\tau = 0$) and bottom of the layer ($\tau = \tau_i^*$) temperatures as the boundary conditions. τ_i^* is the total optical depth of layer i. To find the expression for the downward flux at the bottom of a layer (i.e., at a level) we integrate equation (5) from 0 to τ_i^* and get

$$F^-_{bottom} = F^-_{top} e^{-\tau_i^*/\bar{\mu}} + \pi\left[B_0\left(1 - e^{-\tau_i^*/\bar{\mu}}\right) + B_1\left(\tau_i^* - \bar{\mu} + \bar{\mu}\, e^{-\tau_i^*/\bar{\mu}}\right)\right], \tag{7}$$

where F^-_{top} is the downward flux at the top of the layer, and the *top* and *bottom* subscripts denote the top and bottom edges of the layer, respectively, where down is toward the planetary surface.

[15] For stability reasons, as described later in more detail, the flux in the middle of the layer ($\tau = \tau_i^*/2$) must also be calculated and used in converging the model.

Integrating equation (5) from 0 to $\tau_i^*/2$, we get the downward flux in the middle of the layer:

$$F^-_{midlayer} = F^-_{top} e^{-\tau_i^*/(2\bar{\mu})} + \pi\left[B_0\left(1 - e^{-\tau_i^*/(2\bar{\mu})}\right) + B_1\left(\frac{\tau_i^*}{2} - \bar{\mu} + \bar{\mu}\, e^{-\tau_i^*/(2\bar{\mu})}\right)\right]. \quad (8)$$

[16] The same procedure was used in calculating the upward flux:

$$F^+ = \pi I^+, \quad (9)$$

where I^+ is the upward intensity, given by

$$I^+(\tau, \bar{\mu}) = I^+(\tau_i^*, \bar{\mu})\, e^{-(\tau_i^* - \tau)/\bar{\mu}} + \int_\tau^{\tau_i^*} B(\tau', \bar{\mu})\, e^{-(\tau' - \tau)/\bar{\mu}}\, d\tau'/\bar{\mu}. \quad (10)$$

The Planck function is again approximated as a linear function of τ (equation (6)).

[17] The upward flux at the top of the layer (i.e., integrating from 0 to τ_i^*) is given by

$$F^+_{top} = F^+_{bottom} e^{-\tau_i^*/\bar{\mu}} + \pi\left[B_0\left(1 - e^{-\tau_i^*/\bar{\mu}}\right) + B_1\left(\bar{\mu} - \tau_i^*\, e^{-\tau_i^*/\bar{\mu}} - \bar{\mu}\, e^{-\tau_i^*/\bar{\mu}}\right)\right]. \quad (11)$$

The upward flux in the middle of the layer ($\tau = \tau_i^*/2$) is given by integrating equation (10) from $\tau_i^*/2$ to τ_i^*. After simplifying this gives

$$F^+_{midlayer} = F^+_{bottom} e^{-\tau_i^*/(2\bar{\mu})} + \pi\left[B_0\left(1 - e^{-\tau_i^*/(2\bar{\mu})}\right) + B_1\left(\bar{\mu} + \frac{\tau_i^*}{2} - \tau_i^*\, e^{-\tau_i^*/(2\bar{\mu})} - \bar{\mu}\, e^{-\tau_i^*/(2\bar{\mu})}\right)\right]. \quad (12)$$

[18] Our radiative convective calculation is similar in approach to that of *Pollack et al.* [1987], *McKay et al.* [1989], and *Kasting* [1991]. The radiative fluxes were calculated over a grid extending from the surface to an altitude equivalent to 10^{-9} Pa; the number of layers was set to 30 for all results presented here, but could be varied. It was found that using more than 30 layers resulted in no more than a 0.5% change in the calculated surface temperature change. The layers were about equally spaced in pressure for the bottom 70% of the atmosphere. The albedo in the visible was set to 0.209 in order to give the equilibrium temperature of 212.9 K for the present Mars, as computed by *Pollack et al.* [1987]. The net incoming solar radiation corresponded to the yearly averaged solar flux and was assumed to be deposited at the ground (the atmosphere was assumed transparent in the visible). The outgoing thermal radiation was resolved into 500 spectral intervals from 2 to 2500 cm^{-1}, each with a width of 5 cm^{-1} (except for the first interval); band boundaries were rounded to the nearest interval boundary. All greenhouse gases were assumed to be uniformly mixed in the atmosphere and thus the opacity in each wavelength interval and layer was set proportional to the absorption coefficient for that interval and the pressure difference across the layer.

[19] In order to compute the total upward and downward flux for each level, we first computed these fluxes individually for each spectral interval, and for each term in the exponential sum within the spectral interval ($\mathcal{F}_{\nu,i}$). The opacity for each exponential sum term was calculated using $\tau_i = kN$ where τ_i is the layer opacity, k is the absorption coefficient for the exponential sum term under consideration [m^2 $molecule^{-1}$], and N is the column density of the absorbing gas [molecules m^{-2}]. The total flux for the spectral interval is then given by $\mathcal{F}_\nu = \sum_{i=1}^{n} a_{\nu,i}\mathcal{F}_{\nu,i}$. Summing the flux over all spectral intervals gave the total upward and downward flux for that level.

[20] The computation converged on a steady state solution by requiring that the net upward infrared flux at each layer (the total upward flux minus the total downward flux) balance the net incoming solar flux. The temperatures at the levels were changed proportionately to the residual flux (net up minus net incoming), after the method described by *Pollack and Ohring* [1973], so as to reduce the residual flux to zero. For stability reasons, the flux balance was determined at the mid points of each layer while the temperature was specified at the levels (the layer boundaries) [e.g., *McKay et al.*, 1989]. The computation was iterated upon until there was less than ~0.5% error in the residual flux, with respect to the incoming flux, above the convective zone. This was possible for all partial greenhouse gas pressures of 0.1 Pa or below. For partial pressures of 1 Pa and 10 Pa, the error was as high as 5%.

[21] A convective adjustment was performed if the temperature lapse rate in the layers near the surface exceeded the adiabatic lapse rate. Because the temperatures considered were always less than ~260 K, and thus the saturation vapor pressure of water was negligible, the dry adiabatic lapse rate was used in the calculations. If the adiabatic lapse rate was exceeded in the lowermost layer, then the temperature lapse rate for that level was reset to the adiabatic lapse rate and the radiative balance for the rest of the atmosphere was recalculated using the new boundary condition. The procedure was repeated, each time increasing the thickness of the convective zone by one layer, until a solution was found where the adiabatic lapse rate was not exceeded in any layers and all layers above the convective zone were in radiative equilibrium.

[22] Our numerical scheme was tested by running cases with gray opacities and comparing the level fluxes and resulting temperature profile with the known exact solution. Figure 5 shows comparisons of the multilayer model and the theoretical two-stream approximation results for $\tau = 0.2$, 0.5, 1.0, and 1.5; $\tau = 0.2$ is equivalent to a little less than 0.1 Pa of C_3F_8, and $\tau = 1.5$ is equivalent to a little more than 1 Pa of C_3F_8. Note that there is no convective layer in this calculation. The results match theory very well, especially for higher optical depths. For lower optical depths, the deviation is due to the ground boundary condition: the theoretical result gives the surface discontinuity, while the model smooths the bottom layers as it tries to balance the incoming and outgoing flux at each layer.

[23] The results presented here improve on our previous studies of greenhouse warming on Mars using a simplified one-layer model [*Marinova et al.*, 2000]. The results reported in Table 2 of *Marinova et al.* [2000], for $P_{C_2F_6}$ = 0.01 to 1 Pa, are on average within 27% of the multilayer

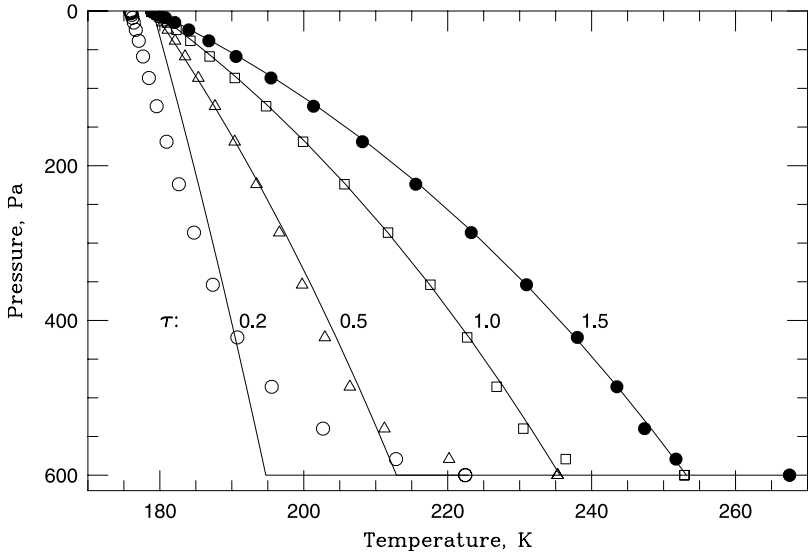

Figure 5. Comparing the multilayer radiative-convective model results (points) with the theoretical results (lines) for a gray atmosphere. The model gives very good results for higher optical depths. For lower optical depths the deviation is the result of the surface discontinuity since the model attempts to balance the fluxes at all levels and create a "smooth" transition.

results listed here. However, this agreement is partly fortuitous, due to an error of a factor of π in the 1-layer flux computer calculations. Note also the typographical error in equation (3) of *Marinova et al.* [2000]: the first plus sign should be a minus sign.

[24] We next compared our results for pure CO_2 atmospheres with the results of *Pollack et al.* [1987]. Our results did not agree, which was not surprising given that we characterized only 3 spectral intervals and only a few bands per spectral interval were used, while high concentrations of CO_2 were modeled. To bring our resulting temperature from CO_2 in alignment with the *Pollack et al.* [1987] results, the CO_2 band opacity was scaled by a constant factor, depending on the CO_2 amount, so as to give the *Pollack et al.* [1987] results. The inclusion of the CO_2 bands, even if artificially scaled, is important due to their interaction with the absorption bands of the other greenhouse gases, as well as for calculating the correct thermal structure of the atmosphere.

4.2. Polar Temperature Calculations

[25] Relating our results to the idea of runaway sublimation of the CO_2 deposits on the planet, we must calculate the polar temperature from the mean annual temperature which is calculated by the radiative-convective model. To do this, we consider the energy balance of the polar regions, taking into account the warming from the artificial greenhouse gases, the incoming solar radiation, and advective heat transport from the equatorial regions:

$$\frac{\sigma T_p^4}{\mathcal{G}} = F_p + F_{adv}, \tag{13}$$

where σ is the Stefan-Boltzmann constant (5.67×10^{-8} J K^{-4} m^{-2} s^{-1}), T_p is the polar temperature, $\mathcal{G}$ is the greenhouse warming factor, F_p is the yearly averaged polar solar flux, and F_{adv} is the heat flux due to advective heat transfer from the equator. F_p can be determined by noting that for the current Mars $F_p = \sigma T_{cap}^4$, where T_{cap} is the polar temperature with no atmospheric warming ($\sim$145 K). T_{cap} was set so that for the current Mars stable equilibrium between the polar temperature and the thickness of the CO_2 atmosphere occurs at 600 Pa. The greenhouse factor $\mathcal{G}$ is defined by *Stephens and Greenwald* [1991] as

$$\mathcal{G} = \left(\frac{T_m}{T_e}\right)^4, \tag{14}$$

where T_m is the mean planetary surface temperature, and T_e is the effective planetary temperature (without any greenhouse gases). The term $1/\mathcal{G}$ can be thought of as the emissivity of the surface and atmospheric column. We assume that the greenhouse factor is the same for the entire planet, specifically that $\mathcal{G}_{mean} = \mathcal{G}_{polar}$.

[26] The advective heat transport is calculated from equation (8) of *Gierasch and Toon* [1973]:

$$F_{adv} = \frac{1}{2} P_{atm}\, \beta \left(T_{eq} - T_p\right), \tag{15}$$

where P_{atm} is the atmospheric pressure [Pa], β is a parameter combining the thermal conduction and convection properties of the atmosphere, here set to $\beta = 1.3 \times 10^{-4}$ m K^{-1} s^{-1} following *Gierasch and Toon* [1973], and T_{eq} is the average equatorial temperature, assumed here to be equivalent to the mean temperature calculated by the radiative-convective model.

[27] Thus our equation for calculating the polar temperature, after substituting for $\mathcal{G}$ and rearranging terms, is

$$T_p = \left[\frac{1}{\sigma}\left(\frac{T_m}{T_e}\right)^4 \left(\sigma T_{cap}^4 + \frac{1}{2} P_{atm}\, \beta \left(T_m - T_p\right)\right)\right]^{\frac{1}{4}}. \tag{16}$$

The equation was solved iteratively.

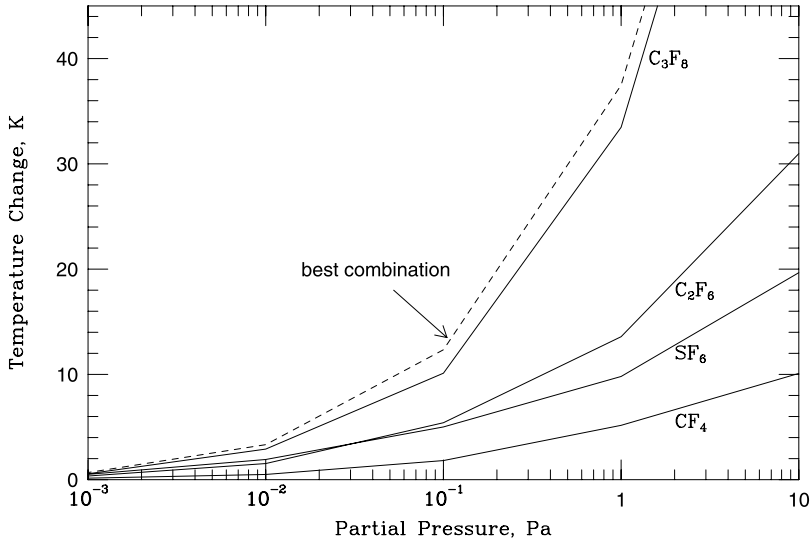

Figure 6. Comparing the warming caused by each fluorine-based gas independently and the best gases combination (dashed line) for the given total greenhouse gas amounts (P_{CO_2} = 600 Pa).

[28] To calculate the amount of greenhouse gases needed to cause Mars to completely outgas its CO_2 inventory, we need to calculate the resulting polar temperature from the presence of various amounts of artificial greenhouse gases and various CO_2 amounts. We first calculated the T_p curve with no artificial greenhouse gases. This is in effect a recalculation of the "Greenhouse" curve in Figure 3 of *McKay et al.* [1991], but equation (16) is preferred because it is physically based on an energy balance. Then we calculated the resulting polar temperature for cases with artificial greenhouse gases.

4.3. Inputs and Outputs

[29] The code takes as input the specified amount of each of the gases, the gas properties file, and the number of layers in the atmosphere, and calculates the resulting surface temperature and atmospheric temperature profile. In addition, the vertical spacing of the layers, the required minimum convergence, and the number of layers can be specified. The gas properties file provides the exponential sum fits for each gas and information about where the gas bands overlap. The model can be further expanded to include the calculation of more greenhouse gases, or to more accurately compute the warming by including clouds, CO_2 release from the regolith and polar caps, etc.

4.4. Computing Multiple Gas Mixtures

[30] The ability to calculate the warming caused by multiple gases required that the overlapping of absorption bands be taken into account. When more than one gas had an absorption band in a wavelength interval, the flux was computed by combining the absorption terms for the gases. This was necessary because we do not have direct measurements of gas combinations.

[31] A scheme was developed to produce a resulting optical depth in the regions with overlapping bands. The optical depth was calculated by noting that an absorption band effectively subdivides each spectral interval into n further sub-bands. The presence of 2 absorption gases in the same spectral interval means the interval is divided into n_1 parts (by the first gas) and then each of these parts is further subdivided into n_2 parts (by the second gas), effectively resulting in $n_3 = n_1 \cdot n_2$ sub-bands within the spectral interval, each with fractional width a_l. Within each sub-band, the effective a and k values are the corresponding product ($a_l = a_i \cdot a_j$, $\sum_{l=1}^{n_3} a_l = 1$) and sum ($k_l = k_i + k_j$). In this representation, the exponential sum approach increases the number of effective wavelengths, but within each of these new effective wavelength intervals the radiative transfer equation is solved directly with the transmission given simply by $e^{-k_l N}$. This procedure can be applied recursively for each additional gas, further subdividing each of the previously subdivided bands. The number of computations (number of sub-bands) is thus the product of the number of exponential terms for the gases.

5. Results and Discussion

[32] The case of most interest is the warming due to the addition of artificial greenhouse gases into the present Martian atmosphere of 600 Pa of CO_2. These results, for the four fluorine-based gases, are shown in Figure 6 and tabulated in Table 1. The results show that there is considerable variability in the greenhouse warming of the four gases listed. C_3F_8 is the strongest followed by C_2F_6 and

Table 1. Temperature Increases Due to Greenhouse Gases on Present Mars[a]

	10^{-4} Pa	10^{-3} Pa	10^{-2} Pa	0.1 Pa	1 Pa	10 Pa
CF_4	0.019 K	0.143 K	0.497 K	1.817 K	5.16 K	10.1 K
C_2F_6	0.052 K	0.348 K	1.53 K	5.41 K	13.6 K	31.0 K
C_3F_8	0.065 K	0.562 K	2.91 K	10.1 K	33.5 K	–
SF_6	0.112 K	0.506 K	1.92 K	5.01 K	9.80 K	19.7 K
Best combination	0.112 K	0.677 K	3.33 K	12.3 K	37.5 K	–

[a] P_{CO_2} = 600 Pa. Cases which resulted in a surface temperature over 260 K were discarded.

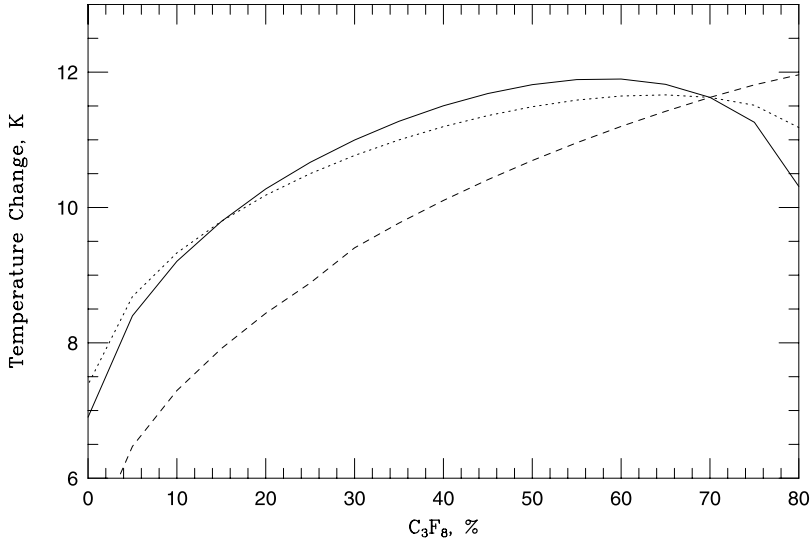

Figure 7. The resulting surface temperature increase for different multigas mixtures, for a total artificial greenhouse gas pressure of 0.1 Pa (P_{CO_2} = 600 Pa). In all cases, two of the gases are set to 10% of the mixture. Dotted line: CF_4 = 10%, C_2F_6 varies, SF_6 = 10%; solid line: CF_4 = 10%, C_2F_6 = 10%, SF_6 varies; dashed line: CF_4 varies, C_2F_6 = 10%, SF_6 = 10%. The results show that when changing the amount of C_2F_6 and SF_6 there is an optimal mixture where all the gases are present, while in changing the amount of CF_4 the highest warming is achieved when no CF_4 is present.

SF_6, with CF_4 being considerably weaker. A nominal 10 K warming on Mars would require ~10 Pa of CF_4, ~0.7 Pa of C_2F_6, ~0.1 Pa of C_3F_8, or ~1 Pa of SF_6. For a surface pressure equal to that on Earth, 1 Pa of a gas corresponds to 10 ppm.

[33] It is interesting to note that of the four gases in Table 1, the largest global warming potential (GWP) in Earth's atmosphere is for SF_6 and not for C_3F_8 [*Houghton et al.*, 2001], by a factor of about 2.6. On Mars the warming results for SF_6 and C_3F_8 are just the opposite of the GWP trends on the Earth, with C_3F_8 causing more than twice as much warming as SF_6. Note that GWP is in essence the warming produced by the gas times the lifetime of the gas; due to the similar lifetimes of SF_6 and C_3F_8 we can compare trends in the GWP values for Earth with the trends in warming values calculated for Mars. The reason for this difference between Earth and Mars may be the absence of H_2O opacity in the present cold Martian atmosphere. As seen in Figure 2, SF_6 has strong bands in the window region where neither CO_2 nor H_2O absorb in Earth's atmosphere. By comparison, C_3F_8 has many of its strong bands in the spectral region where also H_2O absorbs. On Earth these bands are ineffective because of the presence of H_2O while on Mars the virtual absence of H_2O makes these bands important.

5.1. Warming Due to a Gas Mixture

[34] Since the different gases have absorption bands in different parts of the spectrum, it is plausible that a mixture of gases would be much more effective at warming Mars due to a more effective coverage of the entire spectrum. Combinations of gases were considered so as to always add up to a given total partial pressure of greenhouse gases (0.0001 Pa, 0.001 Pa,... to 1 Pa) while varying the percentage contribution of each gas. The case with 10 Pa of greenhouse gases resulted in surface temperatures greater than 260 K and was therefore not included. Figure 7 shows the temperature increase as the relative amounts of the gases are changed for combinations where the total greenhouse gas partial pressure is 0.1 Pa. The plot clearly shows that the highest warming occurs when the mixture is predominantly composed of C_3F_8. As well, it is interesting to note that the resulting warming increases monotonically as the amount of CF_4 decreases, with the highest warming occurring when there is no CF_4 in the mixture, while the inclusion of the other gases is needed to produce the maximum warming.

[35] The use of multiple gases in the warming of Mars has long been considered the most effective method; the results in Figure 6 show that the best combination, given the currently analyzed gases, produces 14%, 22%, and 12% higher temperature increases for amounts of 0.01 Pa, 0.1 Pa, and 1 Pa, respectively. The reason for the small increase is likely due to the great effectiveness of C_3F_8, as it has absorption bands across most of the spectrum (refer to Figure 2). Table 2 shows the combinations and mass fractions of each gas for the best combinations. Such a comparison clearly shows which gases do contribute significantly. Cases with 0.1 Pa of gases or less were converged

Table 2. Gas Percentage Amounts for Producing the Best Combination for Various Total Gas Amounts

	10^{-4}	0.001 Pa	0.01 Pa	0.1 Pa	1 Pa
CF_4	0%	0%	0%	0%	0%
C_2F_6	0%	5%	10%	15%	7.5%
C_3F_8	0%	60%	67.5%	62.5%	82.5%
SF_6	100%	35%	22.5%	22.5%	10%

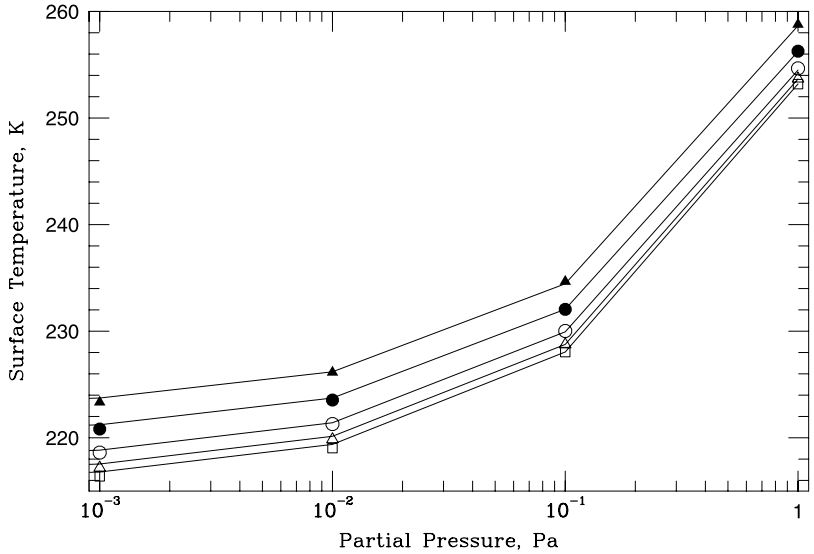

Figure 8. Using a gray atmosphere fit to model the greenhouse warming caused by the best combination of greenhouse gases at different P_{CO_2}. The curves represent different CO_2 atmospheric pressures: 0.6 kPa (Mars today, open squares), 1 kPa (open triangles), 2 kPa (open circles), 5 kPa (solid circles), and 10 kPa (solid triangles).

to less than 0.6% error in residual flux, while for 1 Pa a convergence error of 1.3% was present.

5.2. Gray Opacity Approximation Fits

[36] In order to allow for rapid calculation of the warming caused by greenhouse gases without the need to run the radiative-convective code in its entirety, we computed the effective gray opacity of CO_2 and the fluorine-based greenhouse gases as a function of concentration, and derived simple fits for these results.

[37] For an atmosphere composed purely of CO_2 (600 Pa to 10^4 Pa), using the surface temperature results of *Pollack et al.* [1987], the CO_2 gray opacity can be found using

$$\tau_{CO_2} = 0.004 P_{CO_2}^{0.4551}, \tag{17}$$

where P_{CO_2} is in Pascals. The fit has an error of less than ±3% with respect to the calculated temperature change.

[38] The gray opacity resulting from one of the four greenhouse gases and P_{CO_2} = 600 Pa (τ_{CO_2} = 0.0709) is given by

$$\tau = \tau_{CO_2} + \tau_{gas}, \tag{18}$$

where τ_{gas} is the optical depth of a single artificial greenhouse gas, as calculated by the following relationships:

$$\tau_{CF_4} = 0.137\, P_{CF_4}^{0.682}, \tag{19}$$

$$\tau_{C_2F_6} = 0.3866\, P_{C_2F_6}^{0.502}, \tag{20}$$

$$\tau_{C_3F_8} = 1.095\, P_{C_3F_8}^{0.591}, \tag{21}$$

$$\tau_{SF_6} = 0.27\, P_{SF_6}^{0.391}. \tag{22}$$

All pressures are in Pascals, and the fits are only valid for 600 Pa of CO_2 and up to 1 Pa of the greenhouse gas. These fits are meant to show the general trends and shapes, and fit the data within ±15% of the calculated temperature change for the range 0.01 to 1 Pa for all gases except CF_4, where the errors are up to ±40%. For a more accurate result, the full model must be used.

[39] The optical depth resulting from a combination of CO_2 and the best greenhouse gases combination is given by

$$\tau = \tau_{CO_2} + \tau_{BestGas}, \tag{23}$$

where

$$\tau_{BestGas} = a\,(P_{BestGas})^b, \tag{24}$$

$$a = 4.7 \times 10^{-10}\,(P_{CO_2})^2 + 1.26, \tag{25}$$

$$b = 0.0139\,[\log_{10}(P_{CO_2})]^2 - 0.0955\,\log_{10}(P_{CO_2}) + 0.717. \tag{26}$$

P_{CO_2} and $P_{BestGas}$ are the partial pressures of CO_2 and greenhouse gases, respectively, in Pascals. These fits are valid for $P_{BestGas} \leq 1$ Pa and P_{CO_2} = 600 to 10^4 Pa. Figure 8 shows the calculated values and the respective fits. The fits are accurate to a few percent error in temperature change with respect to present-day Mars temperatures for $P_{BestGas}$ = 0.01 Pa to 1 Pa.

[40] Knowing the optical depth, the resulting surface temperature can then be found using

$$T_s = \left[\frac{F_{sol}\left(1 + \frac{3}{4}\tau\right)}{\sigma}\right]^{\frac{1}{4}}, \tag{27}$$

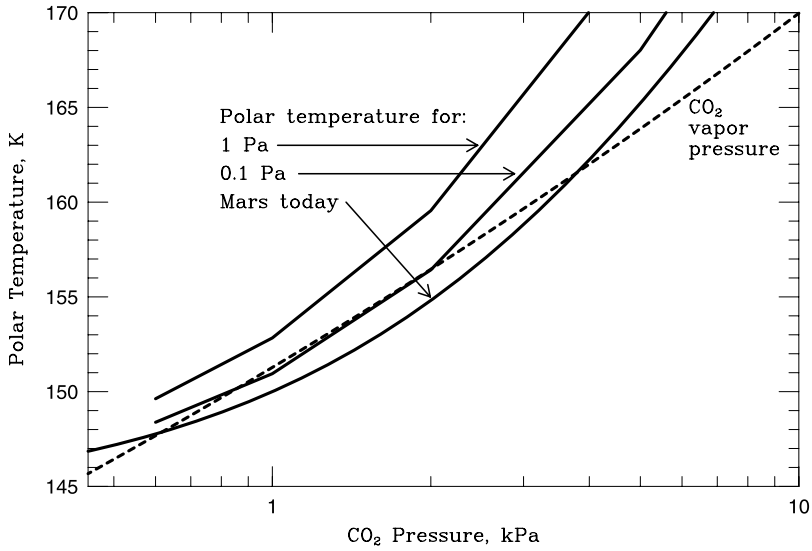

Figure 9. Shifting of the polar temperature versus CO_2 amount equilibrium curve due to different amounts of greenhouse gases in the Martian atmosphere for the best gases combination. About 0.2 Pa of the best combination of greenhouse gases is needed to cause a runaway effect.

where T_s is the resulting surface temperature, F_{sol} is the year-averaged incoming flux at Mars (F_{sol} = 116.5 W m^{-2}), and τ is the optical thickness of the atmosphere as defined above.

5.3. Polar Temperature-Pressure Equilibrium

[41] The stability relationship between polar CO_2 ice and the polar temperature as a function of the atmospheric CO_2 pressure is important in triggering Mars into a runaway greenhouse condition, as discussed above and shown in Figure 1. The fundamental comparison is between the temperature-pressure equilibrium of the CO_2 in the polar caps and the greenhouse temperature-pressure relationship. However, the greenhouse temperature-pressure relationship changes due to the presence of artificial greenhouse gases: the extra warming shifts the greenhouse curve upward in the temperature-pressure diagram. Figure 9 shows the shifted greenhouse curve for different amounts of artificial greenhouse gases, computed using equation (16). As the greenhouse warming is increased by adding artificial greenhouse gases, the equilibrium point A shifts to a higher temperature and CO_2 pressure. A threshold artificial greenhouse warming exists, where the curve will be shifted upward sufficiently as to place the planet into a runaway greenhouse mode, that is, points A and B will merge. Thus it is important to note that our initial estimate of the need for a 20 K warming of the polar regions in order to enter the runaway effect is based on the CO_2 only curve and is an overestimate; a much smaller polar temperature increase will be needed. Note, further, that the temperature critical to the runaway process is the polar temperature, which in this calculation increases with the global mean temperature and also increases with increasing pressure due to advective heat transport. Thus the polar temperature increases faster than the global mean temperature does, assuming the release of CO_2 with the warming of the planet.

[42] Figure 9 shows that about 0.2 Pa of the best mixture (15% C_2F_6, 62.5% C_3F_8, and 22.5% SF_6) of greenhouse gases is needed in order to produce enough warming for Mars to enter a runaway state. For C_3F_8 alone, about 0.4 Pa would be required. As a comparison to the current production of greenhouse fluorine- and chlorine-containing gases on Earth, this represents 25700 times Earth's yearly production. In addition, in order to keep resupplying the gases as they are lost, assuming the lifetimes quoted for the Earth, the yearly production on Mars will need to be about 3 times Earth's current yearly production. As discussed in the Introduction, the lifetimes of these gases could be much longer on Mars, and therefore the loss rate, and corresponding replenishment rate, would be much lower.

6. Conclusion

[43] We have obtained new laboratory measurements of the thermal infrared absorption spectra of artificial greenhouse gases that could be used to warm Mars in order to make it habitable for life in the future. We find that exponential sum fits with one to three terms, depending on the band strength, provide good fits to the bands of these gases. Using these exponential sum fits we have calculated the greenhouse effect for CF_4, C_2F_6, C_3F_8, and SF_6 on present Mars using a spectrally resolved radiative-convective code. On the basis of the results we draw the following conclusions:

[44] 1. The production of fluorine-based gases at levels of 0.1 to 1 Pa is a possible way to increase the mean Mars temperature to the levels necessary to cause the outgassing and evaporation of any available CO_2 ice on Mars.

[45] 2. Of the gases analyzed here, C_3F_8 is the most potent artificial greenhouse gas for use on the present Mars. Since many of its bands overlie those of H_2O, C_3F_8 offsets the fact that the temperature on Mars is so low that H_2O is not present in the atmosphere. A few tenths of a Pascal of C_3F_8 (a few ppm in an Earth-like atmosphere) would result in sufficient warming of Mars to cause complete CO_2 outgassing.

Table A1. Exponential Sum Fit and Intensity Values for CF_4

Wave Number, cm^{-1}	a_i, k_i, m^2 $molecule^{-1}$			Intensity, cm^{-2} atm^{-1}
569–682	0.714, 3.00E-25	0.286, 3.99E-24		2.61
1004–1120	1.000, 7.03E-26			25.18
1190–1334	0.550, 1.57E-25	0.222, 2.48E-22	0.228, 9.64E-24	35.78
1425–1580	0.852, 2.08E-25	0.148, 3.52E-24		3266.12
1624–1749	1.000, 1.26E-25			23.33
1840–1960	0.992, 1.73E-25	0.008, 9.30E-24		4.90
2105–2200	0.802, 1.13E-25	0.198, 3.12E-24		7.07
2440–2630	0.885, 2.61E-25	0.115, 2.41E-24		19.92
3725–3879	1.000, 1.45E-26			0.64

Table A2. Exponential Sum Fit and Intensity Values for C_2F_6

Wave Number, cm^{-1}	a_i, k_i, m^2 $molecule^{-1}$			Intensity, cm^{-2} atm^{-1}
475–580	0.435, 2.42E-24	0.565, 1.42E-25		0.92
660–740	0.510, 1.47E-23	0.490, 2.72E-25		2.70
784–949	1.000, 5.58E-26			0.70
985–1044	0.100, 1.10E-24	0.900, 1.55E-25		9.01
1044–1075	1.000, 1.76E-25			8.75
1075–1160	0.201, 1.86E-22	0.317, 4.50E-25	0.482, 1.94E-23	129.30
1160–1219	0.438, 4.54E-24	0.562, 4.95E-25		5.21
1219–1285	0.280, 7.45E-22	0.330, 4.47E-23	0.390, 2.27E-24	32.76
1285–1410	0.412, 7.24E-24	0.588, 2.49E-25		6.96
1410–1485	0.049, 4.52E-24	0.951, 2.81E-25		10.21
1574–1663	0.107, 3.47E-24	0.893, 3.12E-25		13.93
1663–1795	0.048, 3.72E-24	0.953, 1.67E-25		8.53
1795–1893	0.376, 6.50E-25	0.625, 2.27E-26		107.11
1893–1984	0.101, 9.42E-25	0.899, 1.37E-25		3837.10
2024–2074	0.236, 2.41E-24	0.764, 1.70E-25		37.30
2096–2192	1.000, 3.05E-26			22.54
2309–2398	0.593, 5.21E-26	0.407, 1.07E-24		988.60
2398–2624	0.380, 8.79E-25	0.620, 6.14E-26		1.50
2624–2688	0.401, 2.98E-27	0.599, 8.15E-25		3.72
3636–3745	1.000, 2.18E-26			11.48

Table A3. Exponential Sum Fit and Intensity Values for C_3F_8

Wave Number, cm^{-1}	a_i, k_i, m^2 $molecule^{-1}$			Intensity, cm^{-2} atm^{-1}
425–502	0.455, 8.15E-26	0.545, 8.35E-25		3.32
502–578	0.355, 5.96E-24	0.645, 4.32E-25		798.81
578–641	1.000, 3.50E-25			551.06
641–699	0.744, 3.90E-25	0.256, 3.25E-24		544.30
699–751	0.456, 2.43E-23	0.342, 3.31E-25	0.202, 1.27E-24	10.88
751–826	0.455, 6.10E-26	0.545, 8.30E-25		3088.93
826–900	1.000, 1.53E-25			483.09
900–1069	0.557, 2.79E-25	0.138, 9.99E-23	0.305, 5.89E-24	47.38
1069–1169	0.342, 6.48E-25	0.238, 1.00E-22	0.420, 3.19E-24	6.71
1169–1225	0.535, 6.93E-24	0.465, 7.31E-23		17.23
1225–1322	0.189, 5.58E-22	0.811, 2.49E-23		171.30
1322–1400	0.647, 2.97E-24	0.353, 5.55E-23		10.45
1400–1499	1.000, 4.91E-25			17.32
1499–1669	0.311, 2.48E-25	0.689, 5.84E-25		24.16
1669–1795	1.000, 2.90E-25			11.74
1795–1845	1.000, 2.72E-25			4.05
1845–1901	1.000, 3.27E-25			5.23
1901–1964	1.000, 2.98E-25			6.29
1964–2100	0.130, 7.03E-25	0.870, 1.04E-25		7.38
2100–2155	1.000, 7.44E-26			7.50
2155–2242	1.000, 2.01E-25			1.20
2242–2288	1.000, 2.23E-25			5.64
2288–2386	0.520, 1.38E-25	0.480, 4.58E-25		3.32
2386–2469	1.000, 6.25E-25			8.45
2469–2590	1.000, 5.58E-25			16.96
2590–2702	0.466, 2.72E-26	0.534, 3.64E-25		20.25

Table A4. Exponential Sum Fit and Intensity Values for SF_6

Wave Number, cm^{-1}	a_i, k_i, m^2 $molecule^{-1}$			Intensity, cm^{-2} atm^{-1}
552–649	0.531, 1.22E-25	0.469, 1.73E-23		238.43
769–813	1.000, 1.34E-26			1.72
813–900	0.902, 2.85E-25	0.098, 6.24E-24		14.71
900–961	0.202, 1.06E-21	0.360, 4.69E-25	0.438, 3.13E-23	0.17
961–1010	0.388, 6.58E-25	0.612, 6.43E-24		3655.80
1010–1095	1.000, 4.84E-26			0.44
1095–1149	1.000, 4.13E-26			51.53
1210–1280	0.105, 1.76E-24	0.895, 1.59E-25		1.14
1324–1412	1.000, 6.44E-26			31.00
1412–1474	1.000, 2.46E-26			13.30
1499–1663	0.341, 1.78E-24	0.659, 7.22E-26		0.60
1663–1736	0.275, 2.14E-24	0.725, 6.29E-26		6.21
1736–1776	1.000, 2.68E-26			0.30
2114–2257	1.000, 2.38E-26			0.97

Table A5. Exponential Sum Fit and Intensity Values for CF_2Cl_2

Wave Number, cm^{-1}	a_i, k_i, m^2 $molecule^{-1}$			Intensity, cm^{-2} atm^{-1}
400–529	1.000, 4.09E-26			0.69
604–694	0.680, 1.60E-25	0.320, 5.80E-24		10.04
694–794	1.000, 6.33E-26			24.13
814–959	0.332, 1.08E-22	0.386, 2.66E-25	0.282, 9.16E-24	1.80
1044–1129	0.256, 3.76E-25	0.268, 1.02E-23	0.476, 9.26E-23	41.95
1129–1184	0.360, 9.18E-24	0.640, 7.81E-23		1.49
1184–1264	0.900, 5.32E-25	0.100, 5.60E-24		18.46
1264–1440	0.970, 1.45E-25	0.030, 5.58E-24		750.44
1440–1494	1.000, 5.21E-26			0.55
1494–1605	1.000, 1.12E-25			1163.77
1700–1869	1.000, 1.15E-25			6.17
1949–2083	1.000, 1.49E-26			4.20
2150–2336	0.920, 2.98E-25	0.080, 4.41E-24		1470.04
3236–3401	1.000, 1.53E-26			0.84

Table A6. Exponential Sum Fit and Intensity Values for CF_3Cl

Wave Number, cm^{-1}	a_i, k_i, m^2 $molecule^{-1}$			Intensity, cm^{-2} atm^{-1}
495–660	0.041, 5.54E-24	0.959, 1.57E-25		4.11
734–805	0.499, 1.15E-23	0.501, 1.69E-25		4.75
870–969	1.000, 1.97E-25			2.27
1039–1145	0.317, 1.78E-22	0.339, 3.21E-25	0.344, 1.38E-23	100.55
1145–1280	0.533, 3.33E-24	0.258, 1.90E-22	0.208, 2.03E-25	12.55
1280–1394	0.137, 6.08E-24	0.863, 3.02E-25		1.72
1394–1485	1.000, 8.56E-26			4.79
1485–1610	1.000, 1.15E-25			2.43
1610–1709	1.000, 5.96E-26			0.31
1709–1814	1.000, 7.45E-26			0.40
1841–1915	0.027, 6.12E-24	0.973, 1.58E-25		24.80
1949–2016	0.027, 8.35E-24	0.973, 1.42E-25		2147.94
2173–2262	1.000, 3.72E-26			0.14
2262–2347	0.120, 6.26E-24	0.880, 1.81E-25		1590.39
2347–2487	0.041, 8.59E-24	0.959, 2.17E-25		6.04
2500–2577	1.000, 1.49E-26			0.30
3039–3115	1.000, 6.33E-27			13.64
3448–3558	1.000, 1.19E-26			15.84
3558–3663	1.000, 1.23E-26			0.89

Table A7. Exponential Sum Fit and Intensity Values for CF_3Br

Wave Number, cm^{-1}	a_i, k_i, m^2 $molecule^{-1}$			Intensity, cm^{-2} atm^{-1}
480–617	0.050, 1.95E-24	0.950, 1.55E-25		3.97
617–714	0.117, 2.02E-24	0.883, 1.36E-25		1684.07
714–793	0.715, 2.79E-24	0.099, 5.58E-23	0.186, 8.04E-26	9.04
793–877	1.000, 1.49E-25			1535.61
990–1141	0.283, 1.30E-22	0.415, 2.51E-25	0.302, 1.24E-23	9.08
1141–1251	0.362, 3.96E-24	0.265, 1.84E-22	0.373, 4.11E-25	111.81
1251–1351	0.383, 2.04E-24	0.617, 4.24E-25		28.19
1351–1402	1.000, 2.12E-25			3.10
1402–1447	1.000, 2.23E-25			4.06
1447–1552	1.000, 9.68E-26			3.00
1552–1686	1.000, 5.95E-26			2.89
1686–1782	1.000, 1.08E-25			15.99
1782–1901	1.000, 1.12E-25			3.19
1923–1984	0.051, 1.35E-24	0.949, 1.23E-25		2.94
2109–2232	1.000, 7.81E-26			14.77
2232–2336	0.346, 1.36E-24	0.654, 1.16E-25		2.88
2336–2469	0.109, 1.83E-24	0.891, 2.29E-25		2.27
2469–2538	1.000, 2.60E-26			0.50

[46] 3. SF_6 and C_2F_6 are also potent greenhouse gases causing warming per molecule that is of order $^1/_2$ that of C_3F_8.

[47] 4. Simple gray opacity models can reasonably represent the results of the detailed radiative convective calculation.

Appendix A

[48] We list the identified bands and their ranges, 3-term exponential fits (equation (1)), and band intensities (equation (2)) for CF_4, C_2F_6, C_3F_8, SF_6, CF_2Cl_2, CF_3Cl, and CF_3Br in Tables A1 through A7, respectively. See sections 2 and 3 for a complete description of the data, how the bands were identified, fitting procedure, and band intensity calculations.

[49] **Acknowledgments.** This research was supported by the NASA Astrobiology Program. We thank the reviewers for comments which led to substantial improvements in the paper.

References

Burch, D. E., D. A. Gryvnak, R. R. Patty, and C. E. Bartky (1969), Absorption of infrared radiant energy by CO_2 and H_2O IV. Shapes of collision-broadened CO_2 lines, *J. Opt. Soc. Am.*, *59*(3), 267–280.

Byrne, S., and A. P. Ingersoll (2003), A sublimation model for Martian south polar ice features, *Science*, *299*, 1051–1053.

Fogg, M. J. (1995), *Terraforming: Engineering Planetary Environments*, Soc. of Automotive Eng., Warrendale, Pa.

Gerstell, M. F., J. S. Francisco, Y. L. Yung, C. Boxe, and E. T. Aaltonee (2001), Keeping Mars warm with new super greenhouse gases, *Proc. Natl. Acad. Sci. U. S. A.*, *98*, 2154–2157.

Gierasch, P. J., and O. B. Toon (1973), Atmospheric pressure variation and the climate of Mars, *J. Atmos. Sci.*, *30*, 1502–1508.

Hansen, J., A. Lacis, and M. Prather (1989), Greenhouse effect of chlorofluorocarbons and other trace gases, *J. Geophys. Res.*, *94*(D13), 16,417–16,421.

Houghton, J. T., Y. Ding, D. J. Griggs, M. Noguer, P. J. van der Linden, and D. Xiaosu (Eds.) (2001), *Climate Change 2001: The Scientific Basis: Contribution of Working Group I to the Third Assessment Report of the Intergovernmental Panel on Climate Change (IPCC)*, Cambridge Univ. Press, New York.

Howard, T. N., D. E. Burch, and D. Williams (1956), Infrared transmission of synthetic atmospheres, *J. Opt. Soc. Am.*, *46*(4), 334–338.

Jakosky, B. M., B. G. Henderson, and M. T. Mellon (1995), Chaotic obliquity and the nature of the Martian climate, *J. Geophys. Res.*, *100*, 1579–1584.

Kasting, J. F. (1991), CO_2 condensation and the climate of early Mars, *Icarus*, *94*, 1–13.

Ko, M. K. W., N. D. Sze, W.-C. Wang, G. Shia, A. Goldman, F. J. Murcray, D. G. Murcray, and C. P. Rinsland (1993), Atmospheric sulfur hexafluoride: Sources, sinks and greenhouse warming, *J. Geophys. Res.*, *98*(D6), 10,499–10,507.

Kratz, D. P., M.-D. Chou, M. M.-H. Yan, and C.-H. Ho (1998), Minor trace gas radiative forcing calculations using the k distribution method with one parameter scaling, *J. Geophys. Res.*, *103*(D24), 31,647–31,656.

Lovelock, J. E., and M. Allaby (1984), *The Greening of Mars*, St. Martin's, New York.

Marinova, M. M., C. P. McKay, and H. Hashimoto (2000), Warming Mars using artificial super-greenhouse gases, *J. Br. Interplanet. Soc.*, *53*, 235–240.

McKay, C. P., J. B. Pollack, and R. Courtin (1989), The thermal structure of Titan's atmosphere, *Icarus*, *80*, 23–53.

McKay, C. P., O. B. Toon, and J. F. Kasting (1991), Making Mars habitable, *Nature*, *352*, 489–496.

Mellon, M. T. (1996), Limits on the CO_2 content of the Martian polar deposits, *Icarus*, *124*, 268–279.

Meador, W. E., and W. R. Weaver (1980), Two-stream approximations to radiative transfer in planetary atmospheres: A unified description of existing methods and a new improvement, *J. Atmos. Sci.*, *37*, 630–643.

Pollack, J. B., and G. Ohring (1973), A numerical method for determining the temperature structure of planetary atmospheres, *Icarus*, *19*, 34–42.

Pollack, J. B., J. F. Kasting, S. M. Richardson, and K. Poliakoff (1987), The case for a wet, warm climate on early Mars, *Icarus*, *71*, 203–224.

Pollack, J. B., et al. (1993), Near-infrared light from Venus' nightside: A spectroscopic analysis, *Icarus*, *103*, 1–42.

Ramanathan, V., R. J. Cicerone, H. B. Singh, and J. T. Kiehl (1985), Trace gas trends and their potential role in climate change, *J. Geophys. Res.*, *90*, 5547–5566.

Rodhe, H. (1990), A comparison of the contribution of various gases to the greenhouse effect, *Science*, *248*, 1217–1219.

Roehl, C. M., D. Boglu, C. Brühl, and G. K. Moortgat (1995), Infrared band intensities and global warming potentials of CF_4, C_2F_6, C_3F_8, C_4F_{10}, C_5F_{12}, and C_6F_{14}, *Geophys. Res. Lett.*, *22*(7), 815–818.

Stephens, G. L., and T. J. Greenwald (1991), The Earth's radiation budget and its relation to atmospheric hydrology: 1. Observations of the clear sky greenhouse effect, *J. Geophys. Res.*, *96*(D8), 15,311–15,324.

Sun, Z., and L. Rikus (1999), Improved application of exponential sum fitting transmissions to inhomogeneous atmosphere, *J. Geophys. Res.*, *104*(D6), 6291–6303.

Thomas, G. E., and K. Stamnes (1999), *Radiative Transfer in the Atmosphere and Ocean*, Cambridge Univ. Press, New York.

Toon, O. B., C. P. McKay, T. P. Ackerman, and K. Santhanam (1989), Rapid calculation of radiative heating rates and photodissociation rates in inhomogeneous multiple scattering atmospheres, *J. Geophys. Res.*, *94*(D13), 16,287–16,301.

Varanasi, P., and S. Chudamani (1988), Infrared intensities of some chlorofluorocarbons capable of perturbing the global climate, *J. Geophys. Res.*, *93*(D2), 1666–1668.

H. Hashimoto, Institute of Engineering Mechanics and Systems, University of Tsukuba, Tsukuba, 305-8573, Japan. (hhashi@kz.tsukuba.ac.jp)

M. M. Marinova, California Institute of Technology, MC 150-21, Pasadena, CA 91125, USA. (mmm@caltech.edu)

C. P. McKay, NASA Ames Research Center, MS 245-3, Moffett Field, CA 94035, USA. (cmckay@arc.nasa.gov)